Friction **7**(4): 359–371(2019)
https://doi.org/10.1007/s40544-018-0229-3
ISSN 2223-7690
CN 10-1237/TH
RESEARCH ARTICLE

Boundary element method (BEM) applied to the rough surface contact vs. BEM in computational mechanics

Yang XU*, Robert L. JACKSON
Mechanical Engineering Department, Auburn University, AL 36849, USA
Received: 17 January 2018 / Revised: 17 May 2018 / Accepted: 05 July 2018

Abstract: In the numerical study of rough surfaces in contact problem, the flexible body beneath the roughness is commonly assumed as a half-space or a half-plane. The surface displacement on the boundary, the displacement components and state of stress inside the half-space can be determined through the convolution of the traction and the corresponding influence function in a closed-form. The influence function is often represented by the Boussinesq-Cerruti solution and the Flamant solution for three-dimensional elasticity and plane strain/stress, respectively. In this study, we rigorously show that any numerical model using the above mentioned half-space solution is a special form of the boundary element method (BEM). The boundary integral equations (BIEs) in the BEM is simplified to the Flamant solution when the domain is strictly a half-plane for the plane strain/stress condition. Similarly, the BIE is degraded to the Boussinesq-Cerruti solution if the domain is strictly a half-space. Therefore, the numerical models utilizing these closed-form influence functions are the special BEM where the domain is a half-space (or a half-plane). This analytical work sheds some light on how to accurately simulate the non-half-space contact problem using the BEM.

Keywords: boundary element method; rough surface contact; half-space; half-plane; Flamant solution; Boussinesq-Cerruti solution

1 Introduction

Boundary element method (BEM) is a numerical method used to approximate the solutions of mechanics problems using the boundary integral equation (BIE). It was first used in a paper by Brebbia and Dominguez [1] in 1977. For a linear elastostatic problem, it leads to an integral equation of the tractions and surface displacements over the boundary. Therefore, this method is also known as the boundary integral equation (BIE) method. The development of the computer technology makes BEM a powerful numerical methods and a general-purpose solver for different problems with arbitrary boundary. In the elastostatic problem, the BEM can be described as the Betti's reciprocal theorem (or the Somigliana identity) with the Kelvin's solution (or Mindlin's solution) as the auxiliary solution. By discretizing the boundary, performing the numerical integration over each boundary element and assembling the solution matrix, the unknown (either the surface displacement or traction per node) can be solved numerically from the system of linear equations. The main advantage of BEM for the elastostatic problem is that only the boundary needs to be discretized. The entire domain does not need to be discretized regardless of its size, if the body load is neglected. Additionally, the evaluation of the internal values inside the domain is exact and does not rely on the nodal density of the domain.

The BEM is first applied to the contact mechanics problem by Anderson et al. [2] and later on widely used in many other contact mechanics problems [3–6].

* Corresponding author: Yang XU, E-mail: yang.xu@auburn.edu

Since the conventional BEM[1] results in a dense and unsymmetric matrix which requires $O(N^2)$ memory and $O(N^3)$ operations for solving the system of linear equations using the Gauss elimination [7] where N is the number of nodes. For a reasonable computational time, a conventional BEM may be applied to the problem with 10^5 nodes or less. This is the main reason why the contact interfaces in those work are represented by (piece-wise) simple curves and discretized with few points. In those work, most of the contact domains are finite and two-dimensional. The spatial (three-dimensional) contact needs more boundary nodes and thus longer computational time. Therefore, the axisymmetric domain is commonly studied for the sake of low computational time. This disadvantage may be overcome by the fast multipole BEM [7].

Long before the birth of this numerical method, its fundamental, i.e., the boundary integral equation, has been intensively used by Muskhelishvili [8], Galin [9], Timoshenko and Goodier [10], Gladwell [11], Johnson [12], etc., in the contact mechanics to find the analytical solutions. This is due to the nature of the contact mechanics where most of the interesting solutions (e.g., contact pressure, contact area, surface displacement, etc.,) are on the contact interface (i.e., the boundary). In nearly all those work, the domain is assumed to be a half-space or a half-plane. This is because that the solid contact between bodies is often a local phenomenon so that the dimension of the contact area is negligibly small compared to that of the contacting bodies. There are attempts working on the non-half-space domains (e.g., quarter space [13−16] and thin layer [17]). For an arbitrary boundary, the finite element method (FEM) may be used to calculate the corresponding influence coefficients [18].

Ever since the pioneering work of Conry and Seireg [19] and Kalker and Van Randen [20], a series of similar numerical models [21−49] have been proposed and are dominant in the simulation of rough surface contact. Those models all adopt the same assumption that the flexible bodies of the contact pair are half-spaces or half-planes. For a non-periodic problem, the surface displacement components can be modeled as a convolution of the tractions and the corresponding influence functions. For a non-periodic continuum half-space, the influence function is either the Boussinesq-Cerruti solution (three dimensional elasticity) [42] or Flamant (plane strain/stress condition) [21] solution. For a periodic continuum problem, the influence function is either the Westergarrd solution (plane strain/stress condition) or the Tripp solution [50] (three dimensional elasticity). If the micro-structure of the half-space is considered (e.g., the half-space is composed of lattices), the lattice Green's function can be used as the influence function [41]. In the discretized domain, the surface displacement vector can be calculated by the traction vector multiplied by a discretized influence matrix [42]. The normal boundary condition on the interface follows the Signori inequality (also known as the Kuhn-Tucker condition). Tangential boundary conditions varies with problems and the common ones are full stick, perfect slip and partial slip. These types of numerical models are wildly applied to the purely normal contact [33], sliding contact [40], partial slip [42], rolling contact [47] and adhesive contact [44, 48]. The unknown tractions (e.g., contact pressure and shear stress) are solved iteratively through enforcing the corresponding boundary conditions. This may be done by transforming the contact problem to an equivalent optimization problem and solved by the classic solvers (e.g., the conjugate gradient (CG) method) [37, 46, 47].

In the early days, this type of numerical model is associated with different names, e.g., finite surface element model [21], conventional deformation matrix method [28], moving grid method [28], FFT-based method [33], etc. Starting from the work of Peng and Bhushan [40], this type of numerical methods is commonly accepted as the boundary element method (BEM). The reason lies in the fact that the surface displacement is calculated by the integral equation over the boundary which has a similar manner as the BIE in BEM. Therefore, the numerical models applied to the rough surface contact mentioned above may all be treated as the special BEM where the domain is a half-space. However, a rigorous proof is missing. To distinguish these two models, the so called BEM applied to the rough surface contact is referred to as

[1] The conventional BEM is referred to as those BEM without using fast algorithm.

the special BEM. The other one is referred to as the general BEM. The logic behind this proof is that the boundary integral equation using the Flamant solution and Boussinesq-Cerruti solution as the influence function can be recovered from the general BEM [51] when the domain is a half-space and a half-plane, respectively. The general BEM has recently been applied to the smooth adhesive contact [6] and mixed lubrication where the sub-surface stress is evaluated [52]. Li [52] showed the difference between the sub-surface stress with and without the half-space assumption. As far as we know, the general BEM has rarely been applied to the rough surface contact [52]. This proof can be served as a complimentary material for the BEM community that the half-space problem can be further simplified using more straight-forward integral equation. In the mean time, this study introduces the general BEM to the tribologists to improve the accuracy of a non-half-space problem.

In Section 2, the general BEM of an elastostatic problem with a finite body is briefly discussed. In Section 3, the general BEM is shown to degrade to the special BEM with the Flamant solution as the influence function if the domain is a half-plane. Similarly, in Section 4, the general BEM is shown to degrade to the special BEM where the Boussinesq-Cerruti solution is the influence function if the domain is a half-space.

2 Boundary element method for a finite domain

BEM is a powerful numerical technique used in continuum mechanics, especially for the linear problems. For the elastostatic problem, BEM relies on the Somigliana identity and the fundamental solutions (e.g., the Kelvin and Mindlin solution). If the body load is neglected, only the boundary of the domain needs to be discretized. The internal values of displacement, stress and strain can be accurately determined by the corresponding integral equation. This is a major difference from the finite element method (FEM) which is another popular methodology in the rough surface contact problems [53, 54]. The entire domain in the FEM should be discretized and the accuracies of the internal values rely on the nodal density of the sub-surface.

Three-dimensional elasticity. Consider a finite three-dimensional (3D) domain which is enclosed by the boundary Γ. The domain, Ω, is subjected to the traction vector, $\boldsymbol{p}=[q_x, q_y, p]$, and the surface displacement vector, $\overline{\boldsymbol{u}}=[\overline{u}, \overline{v}, \overline{w}]$, over Γ. For an elastostatic problem, the internal displacement component vector, $\boldsymbol{u}=[u, v, w]$, inside the domain Ω (the boundary Γ is excluded) is expressed by the following boundary integral equation (BIE) in tensor notation [51, 55]:

$$u_i(\boldsymbol{x})=\int_\Gamma u_{ij}^*(\boldsymbol{x},\boldsymbol{\xi})p_j(\boldsymbol{\xi})\mathrm{d}\Gamma(\boldsymbol{\xi})- \int_\Gamma p_{ij}^*(\boldsymbol{x},\boldsymbol{\xi})\overline{u}_j(\boldsymbol{\xi})\mathrm{d}\Gamma(\boldsymbol{\xi}),\ i=1,2,3 \tag{1}$$

which is also known as the Somigliana identity. The source point is $\boldsymbol{x}=[x, y, z]\in\Omega$ and the field point is $\boldsymbol{\xi}=[\xi, \zeta, \eta]\in\Gamma$. The kernels, u_{ij}^* and p_{ij}^*, are the auxiliary (fundamental) solutions of thedisplacement and the traction components at $\boldsymbol{\xi}\in\Gamma$ in an elastic infinite domain due to an point load acting at $\boldsymbol{x}$ (it is commonly known as the Kelvin solution). The explicit forms of the kernels, u_{ij}^* and p_{ij}^*, for three-dimensional elasticity can be found in Eqs. (A7) and (A8) in Appendix A. The kernels are singular when $\boldsymbol{x}\to\boldsymbol{\xi}$. Note that BIEs in Eq. (1) are not singular since $\boldsymbol{\xi}\in\Gamma$ and $\boldsymbol{x}\in\Omega$ (where the boundary Γ is excluded).

Based on the strain-displacement relation and Hooke's law, the internal state of stress σ_{ij} inside Ω can be expressed in a similar manner by the following BIE [51, 55]:

$$\sigma_{ij}(\boldsymbol{x})=\int_\Gamma D_{ijk}^*(\boldsymbol{x},\boldsymbol{\xi})p_k(\boldsymbol{\xi})\mathrm{d}\Gamma(\boldsymbol{\xi})-\int_\Gamma S_{ijk}^*(\boldsymbol{x},\boldsymbol{\xi})\overline{u}_k(\boldsymbol{\xi})\mathrm{d}\Gamma(\boldsymbol{\xi}) \tag{2}$$

where the kernels, D_{ijk}^* and S_{ijk}^*, are given in Eqs. (A11) and (A13).

For a discretized form of Eq. (2) associated with higher order elements (e.g., linear, quadratic, etc.), the nearly singular behavior of sub-surface stress occurs when $\boldsymbol{x}$ is close to the boundary. This is caused by the numerical error introduced by the conventional Gauss quadrature [56]. The distance transformation method [52, 56] may be used to improve the accuracy of sub-surface stresses for these cases. Note that the stress in the left hand side of Eq. (2) *are not singular* if the integrals on the right hand side are solved

analytically. For a discretized form of Eq. (2), non-singular behavior may also be held if the boundary is discretized only by constant elements. This is because integrals over constant elements have closed-form solutions [7].

When $\boldsymbol{x}\to\Gamma$, Eq. (1) can be deduced to the following BIE for the surface displacement:

$$C_{ij}(\boldsymbol{x})\overline{u}_j(\boldsymbol{x})=\int_\Gamma u_{ij}^*(\boldsymbol{x},\boldsymbol{\xi})p_j(\boldsymbol{\xi})\mathrm{d}\Gamma(\boldsymbol{\xi})-\int_\Gamma p_{ij}^*(\boldsymbol{x},\boldsymbol{\xi})\overline{u}_j(\boldsymbol{\xi})\mathrm{d}\Gamma(\boldsymbol{\xi}) \tag{3}$$

where $C_{ij}(\boldsymbol{x})=\frac{1}{2}\delta_{ij}$ if Γ is of class C^1 (continuously or piece-wisely differentiable up to the first order). Otherwise, $C_{ij}(\boldsymbol{x})$ can be determined based on the fact that the rigid body displacement is excluded when the boundary is traction-free. After discretizing the boundary Γ, the above BIE, together with the boundary conditions, can be formed into a system of linear equations. For more details on numerically solving BIE in Eq. (3), readers should refer to the text books [7, 51, 55].

The kernel p_{ij}^* has a strong singularity $O\left(\frac{1}{\varepsilon^2}\right)$ and u_{ij}^* has a weak singularity $O\left(\frac{1}{\varepsilon}\right)$ where $\varepsilon=|\boldsymbol{\xi}-\boldsymbol{x}|$. Thus, the boundary integrals with kernels, p_{ij}^* and u_{ij}^*, in Eq. (3) are in the sense of the *Cauchy principal value*, i.e., in Ref. [51],

$$\int_\Gamma p_{ij}^*(\boldsymbol{x},\boldsymbol{\xi})\overline{u}_j(\boldsymbol{\xi})\mathrm{d}\Gamma(\boldsymbol{\xi})=\int_{\Gamma-\Gamma_\varepsilon} p_{ij}^*(\boldsymbol{x},\boldsymbol{\xi})\overline{u}_j(\boldsymbol{\xi})\mathrm{d}\Gamma(\boldsymbol{\xi}),$$

where Γ_ε is an infinitesimally small surface of radius ε centered about $\boldsymbol{x}$.

Consider a discretized boundry consisting of m line segments (elements): $\Gamma=\{\Gamma_l\,|\,l=1,\ldots,m\}$. In the rough surface contact model, the boundary values are usually assumed to be uniform within each element. In BEM, this type of element is referred to as the constant element. Only one node needs to be placed within each element (commonly at the centroid). Therefore, the group of source nodes and field nodes are: $\{\boldsymbol{x}_k\,|\,k=1,\ldots,m\}$ and $\{\boldsymbol{\xi}_l\,|\,l=1,\ldots,m\}$. Let $\boldsymbol{p}_l=[\tau_x,\tau_y,p]^{\mathrm{T}}$ and $\boldsymbol{u}_l=[u,v,w]^{\mathrm{T}}$ be the traction and surface displacement vectors associated with each field point. Assuming Γ is of class C^1, the discretized form of Eq. (3) is

$$\frac{1}{2}\begin{pmatrix}\boldsymbol{u}_1\\ \vdots\\ \boldsymbol{u}_k\\ \vdots\\ \boldsymbol{u}_m\end{pmatrix}=\begin{pmatrix}\boldsymbol{U}_{11}^* & \cdots & \boldsymbol{U}_{1m}^*\\ \vdots & \boldsymbol{U}_{kl}^* & \vdots\\ \boldsymbol{U}_{m1}^* & \cdots & \boldsymbol{U}_{mm}^*\end{pmatrix}\begin{pmatrix}\boldsymbol{p}_1\\ \vdots\\ \boldsymbol{p}_l\\ \vdots\\ \boldsymbol{p}_m\end{pmatrix}-\begin{pmatrix}\boldsymbol{P}_{11}^* & \cdots & \boldsymbol{P}_{1m}^*\\ \vdots & \boldsymbol{P}_{kl}^* & \vdots\\ \boldsymbol{P}_{m1}^* & \cdots & \boldsymbol{P}_{mm}^*\end{pmatrix}\begin{pmatrix}\boldsymbol{u}_1\\ \vdots\\ \boldsymbol{u}_l\\ \vdots\\ \boldsymbol{u}_m\end{pmatrix} \tag{4}$$

where $\boldsymbol{U}_{kl}^*$ and $\boldsymbol{P}_{kl}^*$ are the influence sub-matrices (3×3) associated with element Γ_l and source point $\boldsymbol{x}_k$. For example:

$$\boldsymbol{U}_{kl}^*=\left[\int_{\Gamma_l} u_{ij}^*(\boldsymbol{x}_k,\boldsymbol{\xi})\mathrm{d}\Gamma(\boldsymbol{\xi}),\quad i,j=1,2,3\right]_{3\times3} \tag{5}$$

After combining the common terms in Eq. (4) and matrix inversion, we have

$$\boldsymbol{u}_k=\sum_{l=1}^{m}\boldsymbol{K}_{kl}\boldsymbol{p}_l,\quad k=1,2,\cdots,m \tag{6}$$

where $\boldsymbol{K}_{kl}$ is the influence sub-matrices (3×3) representing the surface displacement vector at source point $\boldsymbol{x}_i$ due to the unit traction vector acting on Γ_l. When the domain is strictly smooth half-space and problem is purely normal contact, $\boldsymbol{K}_{kl}$ should be the same as the wildly used Love's influence function [12].

Plane strain condition. A finite 3D domain is degraded to a 2D domain over the xy plane where the field and source points are $\boldsymbol{\xi}=[\xi,\zeta]$ and $\boldsymbol{x}=[x,y]$, respectively. Boundary integral equations in Eqs. (1), (2) and (3) are still valid. The traction, surface displacement and internal displacement vectors become $\boldsymbol{p}=[q_x,p]$, $\overline{\boldsymbol{u}}=[\overline{u},\overline{v}]$ and $\boldsymbol{u}=[u,v]$, respectively. The kernels, u_{ij}^*, p_{ij}^*, D_{ijk}^* and S_{ijk}^* for plane strain condition are available in Eqs. (A1), (A2), (A5) and (A6), respectively.

3 Boundary element method for a half-plane problem

In the plane strain condition, consider a half-plane with a flat boundary: $\Gamma=\{(x,y)\,|\,x\in\mathbb{R}^1,y=0\}$, see Fig. 1. Equstions (1) and (3) are still valid [51] in this case where the traction and the surface displacement vectors are $\boldsymbol{p}=[q_x,p]$ and $\overline{\boldsymbol{u}}_i=[\overline{u},\overline{v}]$, respectively.

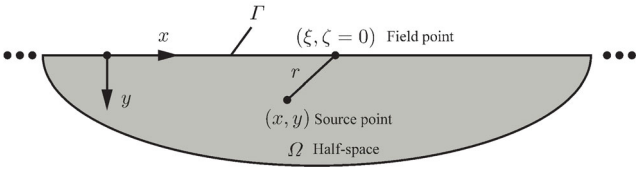

Fig. 1 Schematic representation of a half-plane.

However, Eq. (2) is only valid as long as the state of stress σ_{ij} vanishes at the far end (i.e., $y \to \infty$). This criteria is rarely discussed in the past literatures. The reason is given as follows. The Somigliana identity in Eq. (2) is derived based on the Betti's reciprocal theorem which requires the domain to be bounded by Γ. This implies that the Somigliana identity is only valid for a finite domain. However, Eq. (2) may still be valid for if $\sigma_{ij} r \to 0$ as $r = \sqrt{x^2 + y^2} \to \infty$ [57]. This condition requires the vanishing of the state of stress at the far end which is exactly the criterion shown above. In order to guarantee the stress-free condition at the far end, the average shear and normal tractions over the entire Γ should be strictly zero. Defining a half-plane with the finite boundary: $\Gamma_f = \{(x, y) \mid x \in [-L, L]; y = 0\}$, then the criterion of zero mean traction is:

$$\lim_{L\to\infty} \frac{1}{2L} \int_{\Gamma_f} p_i(x) \mathrm{d}x = 0 \tag{7}$$

For the non-periodic contact where the traction is constrained in one or several finite strip, Eq. (7) is satisfied. If the average shear and normal tractions are not zero (it happens in the periodic contact problem), then the contribution of the average terms on the state of stress should be studied individually.

Due to the simple geometry of the boundary Γ, the following simplification is available for the terms in the Kelvin solution (see Appendix A for more details):

$$\begin{aligned} &\boldsymbol{n} = [0, -1], \quad \boldsymbol{\xi} = [\xi, 0], \quad r = \sqrt{(\xi - x)^2 + y^2}, \\ &r_{,1} = (\xi - x)/r, \quad r_{,2} = -y/r, \quad \partial r/\partial n = y/r \end{aligned} \tag{8}$$

Substituting the above simplification into Eqs. (A1) and (A2), we have the following simplified Kelvin solution:

$$u_{11}^* = \frac{1}{8\pi G(1-\nu)} \left[(3-4\nu) \ln(1/r) + (x-\xi)^2 / r^2 \right],$$

$$u_{22}^* = \frac{1}{8\pi G(1-\nu)} \left[(3-4\nu) \ln(1/r) + y^2 / r^2 \right],$$

$$u_{12}^* = u_{21}^* = \frac{1}{8\pi G(1-\nu)} y(x-\xi)/r^2,$$

$$p_{11}^* = \frac{-1}{4\pi(1-\nu)} \left[(1-2\nu) y r^{-2} + 2y(x-\xi)^2 r^{-4} \right],$$

$$p_{22}^* = \frac{-1}{4\pi(1-\nu)} \left[(1-2\nu) y r^{-2} + 2y^3 r^{-4} \right],$$

$$p_{12}^* = \frac{1}{4\pi(1-\nu)} \left[(1-2\nu)(x-\xi) r^{-2} - 2y^2 (x-\xi) r^{-4} \right],$$

$$p_{21}^* = \frac{-1}{4\pi(1-\nu)} \left[(1-2\nu)(x-\xi) r^{-2} + 2y^2 (x-\xi) r^{-4} \right] \tag{9}$$

It is clear that all the kernels above are functions of $x - \xi$ and y.

Substituting the simplified Kelvin solution listed in Eq. (9) and $y = 0$ into Eq. (3), then it can be splitted into two BIEs[2] for the surface displacement components $\overline{u}$ and $\overline{v}$:

$$\frac{1}{2}\overline{u}(x) = \int_{-\infty}^{\infty} u_{11}^*(x-\xi, 0) q_x(\xi) \mathrm{d}\xi - \int_{-\infty}^{\infty} p_{12}^*(x-\xi, 0) \overline{v}(\xi) \mathrm{d}\xi \tag{10}$$

$$\frac{1}{2}\overline{v}(x) = \int_{-\infty}^{\infty} u_{22}^*(x-\xi, 0) p(\xi) \mathrm{d}\xi - \int_{-\infty}^{\infty} p_{21}^*(x-\xi, 0) \overline{u}(\xi) \mathrm{d}\xi \tag{11}$$

The above set of coupled integral equations can be decoupled using one-dimensional Fourier transform. The explicit form of the one-dimensional Fourier transform pair can be found in Eqs. (B1) and (B2) in Appendix B. Using the convolution law, Eqs. (10) and (11) in the frequency domain are[3]:

$$\frac{1}{2}\overline{U}(k) = U_{11}^*(k, 0) Q_x(k) - P_{12}^*(k, 0) \overline{V}(k) \tag{12}$$

$$\frac{1}{2}\overline{V}(k) = U_{22}^*(k, 0) P(k) - P_{21}^*(k, 0) \overline{U}(k) \tag{13}$$

$U_{11}^*(k, 0)$ can be determined from the closed-form of $U_{11}^*(k, y)|_{y=0}$. For the convenience of derivation, a Fourier transforms table is given in Appendix B, see

[2] The boundary integrals in Eq. (3) are in the sense of Cauchy principle value. Since $p_{ii}^*(x-\xi, 0) = \delta(x-\xi)$, then $\int_{-\infty}^{\infty} p_{ii}^*(x-\xi, 0) \overline{u}_i(\xi) \mathrm{d}\xi = 0$, $i = 1, 2$. $\delta(x-\xi)$ is one-dimensional Dirac function.

[3] Note that the constant term in $U_{11}^*(k, 0)$, i.e., $(x-\xi)^2 / r^2|_{y=0} = 1$ represents the rigid body displacement. This constant term is neglected in the Fourier transform.

Table B1. $P_{12}^*(k,0), U_{22}^*(k,0)$ and $P_{21}^*(k,0)$ are determined similarly. Finally, the closed-forms of $\bar{U}$ and $\bar{V}$ are obtained by solving the system of linear equations in Eqs. (12) and (13):

$$\bar{U}(k)=\frac{1-\nu^2}{\pi E}\frac{1}{|k|}Q_x(k)+\frac{(1-2\nu)(1+\nu)}{2\pi E}\frac{i}{k}P(k) \tag{14}$$

$$\bar{V}(k)=-\frac{(1-2\nu)(1+\nu)}{2\pi E}\frac{i}{k}Q_x(k)+\frac{1-\nu^2}{\pi E}\frac{1}{|k|}P(k) \tag{15}$$

After the inverse Fourier transform of Eqs. (14) and (15), $\bar{u}$ and $\bar{v}$ in the Cartesian coordinates are:

$$\begin{aligned}\bar{u}(x)=&-\frac{2(1-\nu^2)}{\pi E}\int_{-\infty}^{\infty}\ln|x-\xi|\,q_x(\xi)\mathrm{d}\xi-\\&\frac{(1-2\nu)(1+\nu)}{2E}\int_{-\infty}^{\infty}\mathrm{sgn}(x-\xi)p(\xi)\mathrm{d}\xi\end{aligned} \tag{16}$$

$$\begin{aligned}\bar{v}(x)=&\frac{(1-2\nu)(1+\nu)}{2E}\int_{-\infty}^{\infty}\mathrm{sgn}(x-\xi)q_x(\xi)\mathrm{d}\xi-\\&\frac{2(1-\nu^2)}{\pi E}\int_{-\infty}^{\infty}\ln|x-\xi|\,p(\xi)\mathrm{d}\xi\end{aligned} \tag{17}$$

Equations (16) and (17) are exactly the same as the integral forms of the surface displacement using the Flamant solution as the influence functions [12], except for the missing constant terms regarding the rigid body displacement.

Substituting Eqs. (14) and (15) into Eq. (1) in the frequency domain, the displacement components $U(k,y)$ and $V(k,y)$ in the frequency domain are:

$$\begin{aligned}U(k,y)=&\left(\frac{1-\nu^2}{\pi E}\frac{1}{|k|}-\frac{1+\nu}{E}y\right)e^{-2\pi y|k|}Q_x(k)+\\&\left[-\frac{1+\nu}{E}y\,\mathrm{sgn}(k)+\frac{(1+\nu)(1-2\nu)}{2\pi E}\frac{1}{k}\right]ie^{-2\pi y|k|}P(k)\end{aligned} \tag{18}$$

$$\begin{aligned}V(k,y)=&\left[-\frac{1+\nu}{E}y\,\mathrm{sgn}(k)-\right.\\&\left.\frac{(1+\nu)(1-2\nu)}{2\pi E}\frac{1}{k}\right]ie^{-2\pi y|k|}Q_x(k)+\\&\left(\frac{1-\nu^2}{\pi E}\frac{1}{|k|}+\frac{1+\nu}{E}y\right)e^{-2\pi y|k|}P(k)\end{aligned} \tag{19}$$

Sneddon [58] revisited the half-plane problem using the Airy's function and the Fourier transforms. Equations (18) and (19) are the same as those derived by Sneddon [58] if the consistent form of Fourier transform pair is used. Setting $y=0$ in Eqs. (18) and (19), Eqs. (14) and (15) are recovered. After the inverse Fourier transform, the integral forms of the surface displacement using the Flamant solution as the influence function in the Cartesian coordinates are recovered [12, 58].

Applying the Fourier transform to the Hooke's law for the plane strain condition, we have [58]

$$\Sigma_{xx}(k,y)=\frac{E}{(1+\nu)(1-2\nu)}\left[(1-\nu)i2\pi kU(k,y)+\nu\frac{\partial}{\partial\zeta}V(k,y)\right] \tag{20}$$

$$\Sigma_{yy}(k,y)=\frac{E}{(1+\nu)(1-2\nu)}\left[\nu i2\pi kU(k,y)+(1-\nu)\frac{\partial}{\partial y}V(k,y)\right] \tag{21}$$

$$\Sigma_{xy}(k,y)=G\left[\frac{\partial}{\partial y}U(k,y)+i2\pi kV(k,y)\right] \tag{22}$$

Substituting the forms of $U(k,y)$ and $V(k,y)$ given by Eqs. (18) and (19) into Eqs. (20), (21) and (22), we can have the state of stress, Σ_{ij}, in the frequency domain:

$$\begin{aligned}\Sigma_{xx}(k,y)=&i\left[2\,\mathrm{sgn}(k)-2\pi yk\right]e^{-2\pi y|k|}Q_x(k)+\\&(2\pi y|k|-1)e^{-2\pi y|k|}P(k)\end{aligned} \tag{23}$$

$$\Sigma_{yy}(k,y)=i2\pi yke^{-2\pi y|k|}Q_x(k)-(2\pi y|k|+1)e^{-2\pi y|k|}P(k) \tag{24}$$

$$\Sigma_{xy}(k,y)=(2\pi y|k|-1)e^{-2\pi y|k|}Q_x(k)+i2\pi yke^{-2\pi y|k|}P(k) \tag{25}$$

Eqs. (23), (24) and (25) are the same as that derived by Sneddon [58] if a consistent form of the Fourier transform pair is used. Note that $\Sigma_{yy}=\nu(\Sigma_{xx}+\Sigma_{zz})$ for the plane strain condition. After the inverse Fourier transform, the state of stress, σ_{ij}, is represented in the integral form in the Cartesian coordinate using the Flamant solutions as the influence function [12, 58].

In summary, the integral equations using the Flamant solution as the influence functions are a special form of the BEMs in Eqs. (1–3) where the domain is strictly a half-plane.

4 Boundary element method for a half-space problem

Consider a half-space with a flat boundary: $\Gamma=$

$\{(x, y, z) | (x, y) \in \mathbb{R}^2; z = 0\}$, see Fig. 2. Equations (1) and (3) are still valid. Equation (2) is still valid as long as the mean shear and normal tractions on Γ are zero. Defining a half-space with the finite boundary: $\Gamma_f = \{(x, y, z) | x \in [-L_x, L_x], y \in [-L_y, L_y], z = 0\}$, the zero traction criterion can be stated as:

$$\lim_{L_x, L_y \to \infty} \frac{1}{4L_x L_y} \int_{\Gamma_f} p_i(x, y) \mathrm{d}x\mathrm{d}y = 0 \tag{26}$$

A half-space assumption results in the following simplifications of the terms in the Kelvin solutions (see Appendix A for more details):

$$\boldsymbol{n} = [0, 0, -1],\ \boldsymbol{\xi} = [\xi, \zeta, 0],\ \rho = \sqrt{(\xi - x)^2 + (\zeta - y)^2 + z^2},$$
$$\rho_1 = (\xi - x)/\rho,\ \rho_2 = (\zeta - y)/\rho,\ \rho_3 = -z/\rho,\ \partial\rho/\partial n = z/\rho, \tag{27}$$

It is expected that the Kelvin solutions are functions of $\xi - x$, $\zeta - y$ and z. The BIEs in Eqs. (1–3) are the summations of the convolutions of the Kelvin solutions and boundary values (i.e., $\overline{u}_i$ and p_i).

Because of the principle of superposition, the effect on the surface displacement components, $\overline{u}_i$, due to the traction components, $\overline{p}_i$, can be studied individually. Let $q_x \neq 0$ and $q_y = p = 0$ and the corresponding boundary value problem is referred to as the *Cerruti problem*. Substituting the Kelvin solutions shown in Eqs. (A7) and (A8) with the simplifications given in Eq. (27) and $y = 0$ into Eq. (3), then Eq. (3) can be further simplified and the final results are shown below in the two-dimensional frequency domain[4]:

$$\frac{1}{2}\overline{U}(k_x, k_y) - \frac{1-2\nu}{4(1-\nu)}\frac{k_x}{k} i\overline{W}(k_x, k_y) = \frac{1}{16\pi(1-\nu)G}\left[(3-4\nu)\frac{1}{k} + \frac{k_y^2}{k^3}\right] Q_x(k_x, k_y) \tag{28}$$

$$\frac{1}{2}\overline{V}(k_x, k_y) - \frac{1-2\nu}{4(1-\nu)}\frac{k_y}{k} i\overline{W}(k_x, k_y) = \frac{-1}{16\pi(1-\nu)G}\frac{k_x k_y}{k^3} Q_x(k_x, k_y) \tag{29}$$

[4] The boundary integrals in Eq. (3) are in the sense of Cauchy principle value. Since $p_{ii}^*(\xi - x, \zeta - y, 0) = \delta(x - \xi, y - \zeta)$, then $\int_{-\infty}^{\infty}\int_{-\infty}^{\infty} p_{ii}^*(x - \xi, y - \zeta, 0)\overline{u}_i(\xi, \zeta)\mathrm{d}\xi\mathrm{d}\zeta = 0$ where $i = 1, 2, 3$. $\delta(\xi - x, \zeta - y)$ is the two-dimensional Dirac function.

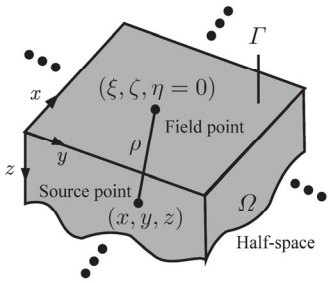

Fig. 2 Schematic representation of a half-space.

$$\frac{1}{2}\overline{W}(k_x, k_y) + \frac{1-2\nu}{4(1-\nu)}\frac{k_x}{k} i\overline{U}(k_x, k_y) + \frac{1-2\nu}{4(1-\nu)}\frac{k_y}{k} i\overline{V}(k_x, k_y) = 0 \tag{30}$$

The information on the two-dimensional Fourier transform pair used in this study can be found in Appendix B. A Fourier transform table is given in Table B1 in Appendix B for the help of deriving Eqs. (28), (29) and (30). Solving the system of linear equations above, we can get the surface displacement components due to the shear traction, q_x, in the frequency domain:

$$\overline{U}(k_x, k_y) = \frac{1}{2\pi G}\left(\frac{1}{k} - \nu\frac{k_x^2}{k^3}\right) Q_x(k_x, k_y) \tag{31}$$

$$\overline{V}(k_x, k_y) = -\frac{\nu}{2\pi G}\frac{k_x k_y}{k^3} Q_x(k_x, k_y) \tag{32}$$

$$\overline{W}(k_x, k_y) = -\frac{1-2\nu}{4\pi G}\frac{ik_x}{k^2} Q_x(k_x, k_y) \tag{33}$$

Using the inverse Fourier transform with the help of Table B1 in Appendix B and the convolution law, the well-known solutions of $\overline{u}_i$ of the Cerruti problem are recovered[12]:

$$\overline{u}(x, y) = \frac{1}{2\pi G}\int_{-\infty}^{\infty}\int \left\{\frac{1-\nu}{\sqrt{(x-\xi)^2 + (y-\zeta)^2}} - \frac{\nu(x-\xi)^2}{\left[(x-\xi)^2 + (y-\zeta)^2\right]^{3/2}}\right\} q_x(\xi, \zeta)\mathrm{d}\xi\mathrm{d}\zeta \tag{34}$$

$$\overline{v}(x, y) = \frac{\nu}{2\pi G}\int_{-\infty}^{\infty}\int \frac{(x-\xi)(y-\zeta)}{\left[(x-\xi)^2 + (y-\zeta)^2\right]^{3/2}} q_x(\xi, \zeta)\mathrm{d}\xi\mathrm{d}\zeta \tag{35}$$

$$\overline{w}(x, y) = \frac{1-2\nu}{4\pi G}\int_{-\infty}^{\infty}\int \frac{x-\xi}{(x-\xi)^2 + (y-\zeta)^2} q_x(\xi, \zeta)\mathrm{d}\xi\mathrm{d}\zeta \tag{36}$$

The results due to the shear traction, q_y, are the same as above if $\bar{u}$ and $\bar{v}$ are interchanged and q_x is replaced by q_y.

Let $p \neq 0$ and $q_x = q_y = 0$, then the corresponding boundary value problem is referred to as the *Boussinesq problem*. The Fourier transform of Eq. (3) results in

$$\frac{1}{2}\bar{U}(k_x,k_y)-\frac{1-2\nu}{4(1-\nu)}\frac{k_x}{k}i\bar{W}(k_x,k_y)=0 \tag{37}$$

$$\frac{1}{2}\bar{V}(k_x,k_y)-\frac{1-2\nu}{4(1-\nu)}\frac{k_y}{k}i\bar{W}(k_x,k_y)=0 \tag{38}$$

$$\begin{aligned}&\frac{1}{2}\bar{W}(k_x,k_y)+\frac{1-2\nu}{4(1-\nu)}\frac{k_x}{k}i\bar{U}(k_x,k_y)+\\&\frac{1-2\nu}{4(1-\nu)}\frac{k_y}{k}i\bar{V}(k_x,k_y)=\frac{3-4\nu}{16\pi(1-\nu)G}\frac{1}{k}P(k_x,k_y)\end{aligned} \tag{39}$$

Solving the above system of linear equations, we have the closed form solution of u_i due to the normal traction, p in the frequency domain:

$$\bar{U}(k_x,k_y)=\frac{1-2\nu}{4\pi G}\frac{ik_x}{k^2}P(k_x,k_y) \tag{40}$$

$$\bar{V}(k_x,k_y)=\frac{1-2\nu}{4\pi G}\frac{ik_y}{k^2}P(k_x,k_y) \tag{41}$$

$$\bar{W}(k_x,k_y)=\frac{1-\nu}{2\pi G}\frac{1}{k}P(k_x,k_y) \tag{42}$$

Using the inverse Fourier transform with the help of Table B1 in Appendix B and the convolution law, the well-known solutions of $\bar{u}_i$ of the Boussinesq problem are recovered [12]:

$$\bar{u}(x,y)=-\frac{1-2\nu}{4\pi G}\iint_{-\infty}^{\infty}\frac{x-\xi}{\left[(x-\xi)^2+(y-\zeta)^2\right]^{3/2}}p(\xi,\zeta)\mathrm{d}\xi\mathrm{d}\zeta \tag{43}$$

$$\bar{v}(x,y)=-\frac{1-2\nu}{4\pi G}\iint_{-\infty}^{\infty}\frac{y-\zeta}{\left[(x-\xi)^2+(y-\zeta)^2\right]^{3/2}}p(\xi,\zeta)\mathrm{d}\xi\mathrm{d}\zeta \tag{44}$$

$$\bar{w}(x,y)=\frac{1-\nu}{2\pi G}\iint_{-\infty}^{\infty}\frac{1}{\sqrt{(x-\xi)^2+(y-\zeta)^2}}p(\xi,\zeta)\mathrm{d}\xi\mathrm{d}\zeta \tag{45}$$

Following the procedures shown in Section 3, the displacement components and the state of stresses inside the domain can be also obtained in the same manner.

In summary, the integral equations using the Boussinesq (Cerruti) solution as the influence functions are a special form of the BEMs in Eqs. (1–3) where the domain is strictly a half-space.

5 Discussions

In this paper, we do not tend to judge how accurate is the special BEM using the Boussinesq-Cerruti/Flamant solutions. The ultimate goal of this theoretical study is to show the relationship between the boundary element method in the community of computational mechanics and the one used in rough surface contact (or more broadly, Tribology). In the previous tribology literatures, this "common sense" has been taken so granted that it was never proved rigorously. The researchers from the community of boundary element method seldom applied BEM to the half-space/quarter or other infinite domains. This history causes a misunderstanding of BEM in many tribology literatures that it can only be applied to the half-space/quarter-space since the corresponding Green's function is available. This paper shows that BEM can be applied not only to the half-space problem, but also to other domains with arbitrary boundary.

In Sections 3 and 4, it is rigorously proved that the so-called BEMs using the Boussinesq-Cerruti (or Flamant) solutions as the influence functions are a special form of the BEM where the domain is strictly a half-space (or half-plane). For the 2D plane strain/stress condition, the Flamant solution is commonly obtained using either the complex variable method [8, 59], the stress function in the polar coordinate [10] or the Airy's function [58]. For the 3D elasticity, the methods include the Boussinesq potentials [12] or the Papkovich-Neuber potentials [60]. This study offers an alternative approach to find the Flamant and Boussinesq-Cerruti solution using the boundary element method.

Therefore, the application of those special BEMs should be restricted to the contact scheme where half-spaces/half-planes are in contact, e.g., the half-space indented by a rigid indenter. However, except for this special contact scenario, there are many schemes where the flexible contact bodies are not exactly half-spaces (e.g., a half-space with a nominally flat rough boundary indented by a rigid flat).

For those cases, the integral equations using the Boussinesq-Cerruti (or Flamant) solutions should be replaced by the BIEs shown in Eqs. (1–3) in order to account for the non-half-space domain. The contact problem is still equivalent to an optimization problem where the classic solver (e.g., Conjugate Gradient method) can still be applied to solve the traction, p_i, and the surface displacement, $\overline{u}_i$. Then, using Eqs. (1) and (2), the displacement and the state of stress inside the domain can be accurately determined. One reason why the Boussinesq-Cerruti (or Flamant) solutions are wildly used on the rough surface contact problems is that the fast algorithm (e.g., the Fast Fourier transform (FFT) [33] and Multi-Level-Multi-Integration (MLMI) [26]) can be applied to accelerate the numerical integration. This benefit no longer exists for Eqs. (1–3). Since the integrals in Eqs. (1–3) are not strictly convolutions, the Fourier transform can no longer be applied, along with the FFT. MLMI [61] significantly reduces the computational time by performing the numerical integration only on the coarse level (with few nodes on it). The final results are approximated through the interpolation between the coarser and finer level. However, it is assumed that the influence coeficient matrix is invariant on all levels. This is not strictly true for a non-half-space (plane) domain, especially when the rough surface exists on the boundary. Therefore, MLMI may not be valid for a non-half-space (plane) problem. This difficulty may be solved by the fast multi-pole method [7].

Recently, BEM is thoroughly discussed in two important papers [62, 63]. The former one is by Müser et al. [62] and it is a summary of the results of a rough surface contact problem challenge initiated in 2016. Among all models, four numerical models are built under the framework of BEM. The Boussinesq solutions are adopted in all four models. Their differences mainly lie in (1) how adhesion is introduced and (2) how to achieve a stable iterative process towards a convergent solution. All the models have good agreement with the experimental results and other methods. This conclusion is valid within the scope that the roughness is relatively smooth.

The latter one [63] is a review paper on the simulation technique in tribology and part of Section 2.2 is dedicated to a brief review of the development of BEM. From the authors' perspective, the BEM mentioned in this review paper is all about the special BEM using the Boussinesq/Cerruti solutions (or other equivalent solutions in the plane strain/stress). The limitations (e.g., large deformation, large sliding, plastic deformation, half-space assumption, etc.) of BEM have been discussed. One of limitations is stated as follows: "Such solutions exist for a limited number of cases and mainly under the assumption that the solid can be locally considered as a flat half-space. These limitations imply a more restrictive field of application for the BEM compared to the FEM, which is a versatile numerical method." In this study, we show theoretically that, at least in the linear elastic problem, BEM is also a versatile numerical method for non half-space problem.

6 Conclusions

In this study, the so-called "BEM" applied to the rough surface contact is rigorously proved to be the special case of the general BEM where the domain is a half-space (or half-plane for plane strain/stress condition). For the plane strain condition, the BIEs in the general BEM results in the well-known Flamant solution. For the three-dimensional elasticity, the same BIE for the relation between the surface displacement and the traction becomes the well-known Bousssinesq (Cerruti) solution if the normal (shear) traction is applied on the boundary alone. The general BEM offers an alternative way to simulate those contact scenarios with a better accuracy where the domain is a non-half-space.

Appendix A The Kelvin solution

The Kelvins solution is the most common fundamental solution used in the elastostatic problem. Consider a linear elastic infinite domain where a unit point load $\boldsymbol{f}$ is applied at the point $\boldsymbol{x}$. The i^{th} component of displacement and traction vector at the point $\boldsymbol{\xi}$ due to the action of the j^{th} component of the unit point load vector are denoted by u_{ij}^* and p_{ij}^*, respectively.

Plane strain. The displacement and the traction can be represented in a tensorial form ($i, j = 1, 2$) [51, 55]

$$u_{ij}^* = \frac{1}{8\pi G(1-\nu)}\left[(3-4\nu)\ln\left(\frac{1}{r}\right)\delta_{ij} + r_{,i}r_{,j}\right] \tag{A1}$$

$$p_{ij}^{*}=\frac{-1}{4\pi(1-\nu)r}\left[(1-2\nu)\left(\frac{\partial r}{\partial n}\delta_{ij}+r_{,j}n_i-r_{,i}n_j\right)+2\frac{\partial r}{\partial n}r_{,i}r_{,j}\right] \tag{A2}$$

where r is the distance between $\boldsymbol{\xi}$ and $\boldsymbol{x}$:

$$r=|\boldsymbol{\xi}-\boldsymbol{x}|=\sqrt{(\xi-x)^2+(\zeta-y)^2} \tag{A3}$$

$r_{,i}=(\xi_i-x_i)/r$ is the derivative of r with respect to ξ_i. $\boldsymbol{n}=[n_x,n_y]$ is the unit normal vector of Γ pointing outwardly. $\partial r/\partial n$ is the normal derivative of r:

$$\frac{\partial r}{\partial n}=\nabla r\cdot\boldsymbol{n}=\sum_{i=1}^{2}r_{,i}n_i \tag{A4}$$

δ_{ij} is the Kronecker delta where $\delta_{ij}=1$ if $i=j$, otherwise $\delta_{ij}=0$.

Other useful forms of the Kelvin solution include D_{ijk}^{*} and S_{ijk}^{*} [51, 55]:

$$D_{ijk}^{*}=\frac{1}{4(1-\nu)r}\left[(1-\nu)(\delta_{ij}r_{,i}+\delta_{ij}r_{,j}-\delta_{ij}r_{,j})+2r_{,i}r_{,j}r_{,k}\right] \tag{A5}$$

$$\begin{aligned}S_{ijk}^{*}=&\frac{G}{2\pi(1-\nu)r^2}\{n_i\left[2\nu r_{,j}r_{,k}+(1-2\nu)\delta_{jk}\right]+\\&n_j\left[2\nu r_{,i}r_{,k}+(1-2\nu)\delta_{ik}\right]+\\&n_k\left[2(1-2\nu)r_{,i}r_{,j}-(1-4\nu)\delta_{ij}\right]+\\&2\frac{\partial r}{\partial n}\left[(1-2\nu)\delta_{ij}r_{,k}+\nu(\delta_{jk}r_{,i}+\delta_{ik}r_{,j})-4r_{,i}r_{,j}r_{,k}\right]\end{aligned} \tag{A6}$$

Three-dimensional elasticity. The displacement and the traction can be represented in a tensorial form ($i,j=1,2,3$) [51, 55]

$$u_{ij}^{*}=\frac{1}{16\pi(1-\nu)G\rho}\left[(3-4\nu)\delta_{ij}+\rho_{,i}\rho_{,j}\right] \tag{A7}$$

$$\begin{aligned}p_{ij}^{*}=&\frac{-1}{8\pi(1-\nu)\rho^2}\left\{[(1-2\nu)\delta_{ij}+3\rho_{,i}\rho_{,j}]\ \frac{\partial\rho}{\partial n}-\right.\\&\left.(1-2\nu)(\rho_{,i}n_j-\rho_{,j}n_i)\right\}\end{aligned} \tag{A8}$$

where ρ is the distance between $\boldsymbol{\xi}$ and $\boldsymbol{x}$:

$$\rho=|\boldsymbol{\xi}-\boldsymbol{x}|=\sqrt{(\xi-x)^2+(\zeta-y)^2+(\eta-z)^2} \tag{A9}$$

and $\rho_{,i}=(\xi_i-x_i)/r$ is the derivative of ρ with respect to ξ_i. $\boldsymbol{n}=[n_x,n_y,n_z]$ is the unit normal vector of Γ pointing outwardly. $\partial\rho/\partial n$ is the normal derivative of ρ:

$$\frac{\partial\rho}{\partial n}=\nabla\rho\cdot\boldsymbol{n}=\sum_{i=1}^{3}\rho_{,i}n_i \tag{A10}$$

Other useful forms of the Kelvin solution include D_{ijk}^{*} and S_{ijk}^{*} [51, 55]:

$$\begin{aligned}D_{ijk}^{*}=&\frac{1}{8\pi(1-\nu)\rho^2}\left[(1-2nu)(\delta_{jk}\rho_{,i}+\delta_{ik}\rho_{,j}-\delta_{ij}\rho_{,k})+\right.\\&\left.3\rho_{,i}\rho_{,j}\rho_{,k}\right]\end{aligned} \tag{A11}$$

$$\begin{aligned}S_{ijk}^{*}=&\frac{G}{4\pi(1-\nu)\rho^3}\left\{n_i\left[3\nu\rho_{,j}\rho_{,k}+(1-2\nu)\delta_{jk}\right]+\right.\\&n_j\left[3\nu\rho_{,i}\rho_{,k}+(1-2\nu)\delta_{ik}\right]+\\&n_k\left[3(1-2\nu)\rho_{,i}\rho_{,j}-(1-4\nu)\delta_{ij}\right]+\\&\left.3\frac{\partial\rho}{\partial n}\left[(1-2\nu)\delta_{ij}\rho_{,k}+\nu(\delta_{jk}\rho_{,i}+\delta_{ik}\rho_{,j})-5\rho_{,i}\rho_{,j}\rho_{,k}\right]\right\}\end{aligned} \tag{A12}$$

Appendix B The Fourier transform table

The one-dimensional Fourier transform pair used in this study is:

$$F(k)=\int_{-\infty}^{\infty}f(\xi)e^{-i2\pi k\xi}\mathrm{d}\xi=\mathcal{F}[f](k) \tag{B1}$$

$$f(\xi)=\int_{-\infty}^{\infty}F(k)e^{i2\pi\xi k}\mathrm{d}k=\mathcal{F}^{-1}[F](x) \tag{B2}$$

A general way of evaluating the Fourier transform and its inverse is using the residual theorem [64]. One-dimensional Fourier transforms frequently used in Section 3 are shown in Table B1.

The two-dimensional Fourier transform pair used in this study is

$$\begin{aligned}F(k_x,k_y)&=\int_{-\infty}^{\infty}\int_{-\infty}^{\infty}f(\xi,\zeta)e^{-i2\pi(k_x\xi+k_y\zeta)}\mathrm{d}\xi\mathrm{d}\zeta\\&=\mathcal{F}[f](k_x,k_y)\end{aligned} \tag{B3}$$

$$\begin{aligned}f(\xi,\zeta)&=\int_{-\infty}^{\infty}\int_{-\infty}^{\infty}F(k_x,k_y)e^{i2\pi(\xi k_x+\zeta k_y)}\mathrm{d}k_x\mathrm{d}k_y\\&=\mathcal{F}^{-1}[F](\xi,\zeta)\end{aligned} \tag{B4}$$

The modulus of (k_x,k_y) is $k=\sqrt{k_x^2+k_y^2}$. Some Fourier transform is evaluated based on the fact that the Fourier transform of the axisymmetric function is the same as the Hankel transform of zero order [58]. Others are evaluated based the some known solution and the derivative law. Some two-dimensional Fourier transforms frequently used in Section 4 are prepared in Table B1.

Table B1 One-dimensional and two-dimensional Fourier transform table. Note that $y \geq 0$.

$f(\xi)$	$F(k)$	$f(\xi,\zeta)$	$F(k_x,k_y)$
$\mathrm{sgn}(\xi)$	$-\frac{i}{\pi k}$	$\frac{1}{\sqrt{\xi^2+\zeta^2}}$	$\frac{1}{k}$
$\ln\left(\frac{1}{\sqrt{\xi^2+y^2}}\right)$	$\frac{1}{2\lvert k\rvert}e^{-2\pi y\lvert k\rvert}$	$-\frac{\xi}{\xi^2+\zeta^2}$	$i\frac{k_x}{k^2}$
$\frac{1}{\xi^2+y^2}$	$\frac{\pi}{y}e^{-2\pi y\lvert k\rvert}$	$-\frac{\xi}{\xi^2+\zeta^2}$	$i\frac{k_y}{k^2}$
$\frac{\xi}{\xi^2+y^2}$	$-i\pi\mathrm{sgn}(k)e^{-2\pi y\lvert k\rvert}$	$\frac{1}{\sqrt{\xi^2+\zeta^2}}-\frac{\xi^2}{(\xi^2+\zeta^2)^{3/2}}$	$\frac{k_x^2}{k^3}$
$\frac{1}{(\xi^2+y^2)^2}$	$\frac{\pi}{2}\frac{1}{y^3}(1+2\pi yk)e^{-2\pi y\lvert k\rvert}$	$\frac{1}{\sqrt{\xi^2+\zeta^2}}-\frac{\zeta^2}{(\xi^2+\zeta^2)^{3/2}}$	$\frac{k_y^2}{k^3}$
$\frac{\xi}{(\xi^2+y^2)^2}$	$-i\pi^2k\frac{1}{y}e^{-2\pi y\lvert k\rvert}$	$-\frac{\xi\zeta}{(\xi^2+\zeta^2)^{3/2}}$	$\frac{k_xk_y}{k^3}$
$\frac{\xi^2}{(\xi^2+y^2)^2}$	$\frac{\pi}{2y}(1-2\pi y\lvert k\rvert)e^{-2\pi y\lvert k\rvert}$		
$\frac{\xi^3}{(\xi^2+y^2)^2}$	$-i\pi\mathrm{sgn}(k)(1-\pi y\lvert k\rvert)e^{-2\pi y\lvert k\rvert}$		

References

[1] Brebbia C A, Dominguez J. Boundary element methods for potential problems. *Appl Math Modell* **1**(7): 372–378 (1977)

[2] Andersson T, Fredriksson B, Allan-Persson B G. The boundary element method applied to two-dimensional contact problems. In *New developments in Boundary Element Methods*. Brebbia C A, Ed. Southampton: CML Publishers, 1980.

[3] Karami G. *A Boundary Element Method for Two-Dimensional Contact Problems*. Berlin (Germany): Springer-Verlag, 1989.

[4] Man K W. *Contact Mechanics using Boundary Elements*. Southampton (UK): Computational Mechanics Inc., 1994.

[5] Dargush G F, Soom A. Contact modeling in boundary element analysis including the simulation of thermomechanical wear. *Tribol Int* **100**: 360–370 (2016)

[6] Wu J J, Lin Y J. Boundary element analyses on the adhesive contact between an elastic sphere and a rigid half-space. *Eng Anal Bound Elem* **74**: 61–69 (2017)

[7] Liu Y J. Fast Multipole Boundary Element Method: Theory and Applications in Engineering. Cambridge (UK): Cambridge University Press, 2009.

[8] Muskhelishvili N I. *Some Basic Problems of the Mathematical Theory of Elasticity*. 3rd ed. Moscow: P. Noordhoff, 1949.

[9] Galin L A. *Contact Problems in the Theory of Elasticity*. Moscow: Gostehizdat, 1953.

[10] Timoshenko S P, Goodier J N. *Theory of Elasticity*. 3rd ed. New York (USA): McGraw-Hill, 1970.

[11] Gladwell G M L. *Contact Problems in the Classical Theory of Elasticity*. Alphen aan den Rijn (Netherlands): Sijthoff and Noordhoff, 1980.

[12] Johnson K L. *Contact Mechanics*. Cambridge (UK): Cambridge University Press, 1987.

[13] Hetényi M. A method of solution for the elastic quarter-plane. *J Appl Mech* **27**(2): 289–296 (1960)

[14] Hetényi M. A general solution for the elastic quarter space. *J Appl Mech* **37**(1): 70–76 (1970)

[15] Keer L M, Lee J C, Mura T. A contact problem for the elastic quarter space. *Int J Solids Struct* **20**(5): 513–524 (1984)

[16] Wang W, Guo L, Wong P L, Zhang Z M. Surface normal deformation in elastic quarter-space. *Tribol Int* **114**: 358–364 (2017)

[17] Carbone G, Mangialardi L. Analysis of the adhesive contact of confined layers by using a Green's function approach. *J Mech Phys Solids* **56**(2): 684–706 (2008)

[18] Vollebregt E, Segal G. Solving conformal wheel-rail rolling contact problems. *Vehicle Syst Dyn* **52**(S1): 455–468 (2014)

[19] Conry T F, Seireg A. A mathematical programming method for design of elastic bodies in contact. *J Appl Mech* **38**(2): 387–392 (1971)

[20] Kalker J J, Van Randen Y. A minimum principle for frictionless elastic contact with application to non-Hertzian half-space contact problems. *J Eng Math* **6**(2): 193–206 (1972)

[21] Francis H A. A finite surface element model for plane-strain elastic contact. *Wear* **76**(2): 221–245 (1982)

[22] Lai W T, Cheng H S. Computer simulation of elastic rough contacts. *ASLE Trans* **28**(2): 172–180 (1985)

[23] Johnson K L, Greenwood J A, Higginson J G. The contact of elastic regular wavy surfaces. *Int J Mech Sci* **27**(6): 383–396 (1985)

[24] Webster M N, Sayles R S. A numerical model for the elastic frictionless contact of real rough surfaces. *J Tribol* **108**(3): 314–320 (1986)

[25] Seabra J, Berthe D. Influence of surface waviness and roughness on the normal pressure distribution in the Hertzian contact. *J Tribol* **109**(3): 462–469 (1987)

[26] Lubrecht A A, Ioannides E. A fast solution of the dry contact problem and the associated sub-surface stress field, using multilevel techniques. *J Tribol* **113**(1): 128–133 (1991)

[27] Ju Y Q, Zheng L Q. A full numerical solution for the elastic contact of three-dimensional real rough surfaces. *Wear* **157**(1): 151–161 (1992)

[28] Ren N, Lee S C. Contact simulation of three-dimensional rough surfaces using moving grid method. *J Tribol* **115**(4): 597–601 (1993)

[29] Snidle R W, Evans H P. A simple method of elastic contact simulation. *Proc Inst Mech Eng, Part J: J Eng Tribol* **208**(4): 291–293 (1994)

[30] Mayeur C, Sainsot P, Flamand L. A numerical elastoplastic model for rough contact. *J Tribol* **117**(3): 422–429 (1995)

[31] Tian X F, Bhushan B. A numerical three-dimensional model for the contact of rough surfaces by variational principle. *J Tribol* **118**(1): 33–42 (1996)

[32] Ju Y, Farris T N. Spectral analysis of two-dimensional contact problems. *J Tribol* **118**(2): 320–328 (1996)

[33] Stanley H M, Kato T. An FFT-based method for rough surface contact. *J Tribol* **119**(3): 481–485 (1997)

[34] Nogi T, Kato T. Influence of a hard surface layer on the limit of elastic contact-Part I: Analysis using a real surface model. *J Tribol* **119**(3): 493–500 (1997)

[35] Borri-Brunetto M, Carpinteri A, Chiaia B. Lacunarity of the contact domain between elastic bodies with rough boundaries: Numerical analysis and scale effects. In *Probamat-21st Century: Probabilities and Materials*. Frantziskonis G N, Ed. Dordrecht: Springer, 1998: 45–64.

[36] Hu Y Z, Barber G C, Zhu D. Numerical analysis for the elastic contact of real rough surfaces. *Tribol Trans* **42**(3): 443–452 (1999)

[37] Polonsky I A, Keer L M. A numerical method for solving rough contact problems based on the multi-level multi-summation and conjugate gradient techniques. *Wear* **231**(2): 206–219 (1999)

[38] Liu S B, Wang Q, Liu G. A versatile method of discrete convolution and FFT (DC-FFT) for contact analyses. *Wear* **243**(1–2): 101–111 (2000)

[39] Jacq C, Nélias D, Lormand G, Girodin D. Development of a three-dimensional semi-analytical elastic-plastic contact code. *J Tribol* **124**(4): 653–667 (2002)

[40] Peng W, Bhushan B. Transient analysis of sliding contact of layered elastic/plastic solids with rough surfaces. *Microsyst Technol* **9**(5): 340–345 (2003)

[41] Campaná C, Müser M H. Practical Green's function approach to the simulation of elastic semi-infinite solids. *Phys Rev B* **74**(7): 075420 (2006)

[42] Willner K. Fully coupled frictional contact using elastic halfspace theory. *J Tribol* **130**(3): 031405 (2008)

[43] Putignano C, Afferrante L, Carbone G, Demelio G. A new efficient numerical method for contact mechanics of rough surfaces. *Int J Solids Struct* **49**(2): 338–343 (2012)

[44] Medina S, Dini D. A numerical model for the deterministic analysis of adhesive rough contacts down to the nano-scale. *Int J Solids Struct* **51**(14): 2620–2632 (2014)

[45] Yastrebov V A, Anciaux G, Molinari J F. From infinitesimal to full contact between rough surfaces: Evolution of the contact area. *Int J Solids Struct* **52**: 83–102 (2015)

[46] Bemporad A, Paggi M. Optimization algorithms for the solution of the frictionless normal contact between rough surfaces. *Int J Solids Struct* **69–70**: 94–105 (2015)

[47] Xi Y H, Almqvist A, Shi Y J, Mao J H, Larsson R. A complementarity problem-based solution procedure for 2D steady-state rolling contacts with dry friction. *Tribol Trans* **59**(6): 1031–1038 (2016)

[48] Bazrafshan M, de Rooij M B, Valefi M, Schipper D J. Numerical method for the adhesive normal contact analysis based on a Dugdale approximation. *Tribol Int* **112**: 117–128 (2017)

[49] Xu Y, Jackson R L. Statistical models of nearly complete elastic rough surface contact-comparison with numerical solutions. *Tribol Int* **105**: 274–291 (2017)

[50] Tripp J H, Van Kuilenburg J, Morales-Espejel G E, Lugt P M. Frequency response functions and rough surface stress analysis. *Tribol Trans* **46**(3): 376–382 (2003)

[51] Brebbia C A, Telles J C F, Wrobel L C. *Boundary Element*

Techniques: Theory and Applications in Engineering. Berlin (Germany): Springer-Verlag, 1984.

[52] Li S. A boundary element model for near surface contact stresses of rough surfaces. *Comput Mech* **54**(3): 833–846 (2014)

[53] Hyun S, Pei L, Molinari J F, Robbins M O. Finite-element analysis of contact between elastic self-affine surfaces. *Phys Rev E* **70**(2): 026117 (2004)

[54] Yastrebov V A, Durand J, Proudhon H, Cailletaud G. Rough surface contact analysis by means of the finite element method and of a new reduced model. *CR Mécanique* **339**(7–8): 473–490 (2011)

[55] Becker A A. *The Boundary Element Method in Engineering: A Complete Course*. New York (USA): McGraw-Hill Companies, 1992.

[56] Ma H, Kamiya N. Distance transformation for the numerical evaluation of near singular boundary integrals with various kernels in boundary element method. *Eng Anal Bound Elem* **26**(4): 329–339 (2002)

[57] Sternberg E. On Saint-Venant's principle. *Quart Appl Math* **11**(4): 393–402 (1954)

[58] Sneddon I N. *The Use of Transform Methods in Elasticity*. Air Force Office of Scientific Research, United States Air Force, 1964.

[59] Cai H T, Lu J K. *Mathematical Theory in Periodic Plane Elasticity*. Newark (USA): Gordon and Breach Science Publishers, 2000.

[60] Barber J R. *Elasticity*. Dordrecht (Netherlands): Kluwer Academic Publishers, 1992.

[61] Brandt A, Lubrecht A A. Multilevel matrix multiplication and fast solution of integral equations. *J Comput Phys* **90**(2): 348–370 (1990)

[62] Müser M H, Dapp W B, Bugnicourt R, Sainsot P, Lesaffre N, Lubrecht T A, Persson B N J, Harris K, Bennett A, Schulze K, et al. Meeting the contact-mechanics challenge. *Tribol Lett* **65**(4): 118 (2017)

[63] Vakis A I, Yastrebov V A, Scheibert J, Nicola L, Dini D, Minfray C, Almqvist A, Paggi M, Lee S, Limbert G, et al. Modeling and simulation in tribology across scales: An overview. *Tribol Int* **125**: 169–199 (2018)

[64] Pinkus A, Zafrany S. *Fourier Series and Integral Transforms*. Cambridge (UK): Cambridge University Press, 1997.

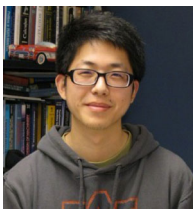

Yang XU. He is a research engineer at Caterpillar Inc. He received his M.S and Ph.D. degrees in mechanical engineering at Auburn University, AL, USA. He has research interests in the area of rough surface contact using analytical, numerical and experimental methodologies, lubrication modeling, and surface metrology.

Robert L. JACKSON. He is the director of the Tribology Program and a professor of mechanical engineering at Auburn University. He received his PhD degree in mechanical engineering, at the Georgia Institute of Technology in Atlanta, GA, USA. He has research interests in the areas of rough surface contact mechanics, contact resistance, multiphysics modeling, hydrodynamic lubrication, and nanoparticle lubricant additives. In 2012, Prof. Jackson also initiated one of the first undergraduate minors in the field of Tribology. Prof. Jackson received the 2011 ASME Burt L. Newkirk Award for notable contributions to the field of Tribology as indicated by significant publications before reaching the age of 40, the 2009 STLE Captain Alfred E. Hunt Memorial Award for the best paper in the field of lubrication, and the 2009 Shobert Paper Award at the Holm Conference on Electrical Contacts. He was also named the best reviewer for the ASME Journal of Tribology in 2008 and 2009.